Electrospinning of Cellulose Benzyl Carbamates for Enantioselective Membrane Filtration

Steve Nono-tagne, Thomas Heinze, Martin Gericke, Issei Otsuka

RESEARCH ARTICLE

Macromolecular Bioscience
www.mbs-journal.de

Electrospinning of Cellulose Benzyl Carbamates for Enantioselective Membrane Filtration

Steve Nono-Tagne, Thomas Heinze, Martin Gericke, and Issei Otsuka**

Electrospun nanofibrous membranes made of chiral selectors (CSs) have shown their potential for efficient chiral resolutions via filtrations. It is thus of great importance to expand the number of electrospun membranes made of various CSs for the resolution of a wide range of chiral compounds. Here, the electrospinning of two benzyl carbamate derivatives of cellulose, namely cellulose benzyl carbamate (CBzC) and cellulose 4-chlorobenzyl carbamate (CCBzC), to form a new type of enantioselective membranes for chiral resolutions of racemic compounds, is reported. The morphology of the electrospun membranes is studied by optical microscopy and scanning electron microscopy in relation to the electrospinning process parameters. Liquid-liquid permeation experiments of the racemic compounds, (*R*,*S*)-1-(1-naphthyl)ethanol ((*R*,*S*)-NET), (*R*,*S*)-1,1′-bi-2-naphtol ((*R*,*S*)-BNP), (*R*,*S*)-naproxen ((*R*,*S*)-NAP), and (*R*,*S*)-benzoin ((*R*,*S*)-BNZ) through the membranes demonstrate preferable permeations of (*R*)- or (*S*)-enantiomers depending on the combinations between the CSs and the racemates. Molecular docking simulations indicate the differences in the binding type, number, and free energies between the CSs and the enantiomers.

1. Introduction

Over the last decades, there has been significant progress in enantioseparation technologies due to the increasing demand for optically pure chemicals in pharmaceuticals, agrochemicals, and other industries.[1,2] Conventional methods for obtaining optically pure chiral substances include chromatographic separation,[3] kinetic resolution,[4] and crystallization.[5] Chromatography, while widely used, often suffers from high operational costs, energy demands, and limited scalability.[6] Kinetic resolution, although effective, usually requires specific catalysts and generates substantial waste due to incomplete conversion.[7] Crystallization technique is characterized of long processing times and limited to molecules that can form conglomerates.[5] On the other hand, membrane-based separation technologies are emerging as a compelling alternative offering several advantages including lower cost, reduced energy consumption, simpler equipment, lower environmental impact, and easier scalability to industrial production, making it a highly promising method for large-scale chiral separation.[8,9] Currently, a wide variety of membranes have been developed, utilizing materials such as polymers, carbon nanomaterials, metal–organic frameworks (MOFs), and other inorganic compounds. Membranes composed of biopolymers such as cellulose and amylose are attractive for chiral separation as some of these materials possess inherent chiral recognition sites, allowing for direct use. In many cases, to induce the chiral selectivity of achiral polymer membranes, various chiral selectors such as cyclodextrins, amino acids, and proteins are introduced through chemical modification, molecular imprinting, or surface grafting techniques.[6] These selectors introduce a number of chiral recognition sites on the membrane, significantly improving separation efficiency. Fabrication methods for these chiral membranes include techniques such as spin coating, dipping, surface grafting, interfacial polymerization, and phase inversion. However, electrospinning stands out for its unparalleled simplicity and scalability, making it suitable for industrial membrane filtration systems.[10]

Electrospun nanofibrous filters have structural advantages for membrane separations thanks to their high surface area to volume ratio due to small fiber diameters ranging from several nanometers to a few micrometers as well as their porous nonwoven structures.[11] These characteristics allow large surface interactions between the filters and the separating molecules as well as good permeation flux.[12] Therefore, membrane separations of chiral molecules using electrospun nanofibrous filters have been explored since the 2000s by imprinting enantiomerically pure amino acid derivatives as chiral selectors (CSs) into achiral electrospun nanofibrous scaffolds[13–15] and by electrospinning of chiral polysaccharides and their derivatives[16–18]

S. Nono-Tagne, I. Otsuka
Univ. Grenoble Alpes
CNRS
CERMAV
Grenoble 38000, France
E-mail: issei.otsuka@cermav.cnrs.fr
T. Heinze, M. Gericke
Institute of Organic Chemistry and Macromolecular Chemistry
Friedrich-Schiller-University Jena
Humboldtstr 10, 07743 Jena, Germany
E-mail: martin.gericke@uni-jena.de

The ORCID identification number(s) for the author(s) of this article can be found under https://doi.org/10.1002/mabi.202400415

DOI: 10.1002/mabi.202400415

to form enantioselective membranes. Recently, we reported a new type of enantioselective membrane purely made of cellulose 3,5-dimethylphenyl carbamate (CDMPC), one of the most popular CSs used for chiral resolutions by high-performance liquid chromatography (HPLC).[19,20] These studies focused on the electrospinning of the CDMPCs synthesized from cellulose of different origins having various degrees of polymerizations to form self-standing nanofibrous membranes. We demonstrated enantioselective permeations of a model racemic compound (*R*,*S*)-1-(1-naphthyl)ethanol ((*R*,*S*)-NET) through the membranes and its simulations using a molecular docking model as a proof of concept for efficient chiral resolutions. However, our findings are limited to the chiral resolution of one single racemic compound and the CS. It is thus of great importance to expand the options for using electrospun membranes made of various CSs for resolutions of a wide range of chiral compounds.

To date, the most reliable and widely used technique for chiral resolutions of practically useful chiral compounds such as pharmaceuticals and pesticides is chromatographic separation by HPLC. Polysaccharides and their derivatives are either physically coated or chemically immobilized on silica gel and packed in chromatography columns as chiral stationary phases (CSPs) for HPLC. Hesse and Hagel first discovered the high chiral recognition property of microcrystalline cellulose triacetate of some racemic compounds in 1973.[21] Since 1984, Okamoto and coworkers have reported a variety of polysaccharide derivatives as CSPs.[22–24] Notably, phenyl carbamate derivatives of cellulose and amylose such as CDMPC and amylose 3,5-dimethylphenyl carbamate (ADMPC) exhibit high chiral recognition of a broad range of racemic compounds. The recognition abilities of these derivatives are significantly affected by the substituent on the phenyl groups such as halogens and alkyl groups.[25,26] On the contrary, the chiral recognition properties of benzyl carbamate derivatives of cellulose and amylose that have one methylene spacer between the phenyl groups and the carbamate bonds are relatively less studied.[27] A reason for this might be the limited availability of suitable isocyanate reagents. Thus, new synthesis approaches are desired.

Polysaccharide carbamates are conventionally prepared by conversion of the biopolymers with highly reactive isocyanates. Recently, a new modular synthesis approach for obtaining polysaccharide carbamates has been proposed in which activated aryl carbonates are employed.[28–30] These compounds that can be prepared with high yields react with aliphatic amines to yield functional polysaccharide carbamates. The advantages of this two-step synthesis over the use of isocyanates are i) less rigorous reaction conditions, which allow for a better control over the molecular structure, ii) a much broader structural diversity because a large variety of commercially available amines can be used instead of a limited selection of isocyanates. A broad variety of functional polysaccharide carbamates and even mixed carbamates has been synthesized by this approach.[28–30] Moreover, it has also been used to prepare cellulose-based CSs for the use as the CSPs in the columns for HPLC.[31,32] It is hypothesized that i) tailored polysaccharide carbamates prepared through this modular approach can be shaped into nanofibers using electrospinning and that ii) membranes formed from these fibers can be used for the separation of chiral compounds.

The aims of this study are i) to synthesize two aromatic cellulose derivatives, namely cellulose benzyl carbamate (CBzC) and cellulose 4-chlorobenzyl carbamate (CCBzC), through a modular approach, ii) to form self-standing nanofibrous membranes of the compounds by electrospinning, iii) to study chiral separation of several racemic compounds, and iv) to study the interaction of the chiral compounds with the two cellulose derivatives by molecular docking simulations.

2. Results and Discussion

2.1. Synthesis of the Benzyl Carbamate Derivatives of Cellulose as the CSs

The first task of this work was the synthesis of aromatic cellulose carbamate derivatives with benzyl moieties. Benzyl isocyanates can potentially be used for the synthesis, but these compounds are rather hazardous and expensive. Thus, a modular synthesis approach was employed in which cellulose phenyl carbonate (CPhC) was used as an activated starting compound (**Figure 1**). This compound can be further converted with a broad variety of aliphatic amines to obtain functional cellulose carbamates.[29,30] In this work, two aromatic cellulose derivatives, namely CBzC and CCBzC, were prepared. For this purpose, CPhC with a high degree of substitution (DS) value of 2.88 was synthesized homogeneously in an ionic liquid with pyridine as co-solvent according to a previously reported procedure.[30,33] Pyridine is used in this reaction because i) it reduces the viscosity of the reaction mixture and facilitates efficient stirring and ii) it acts as scavenger for HCl that is formed in this reaction. The products were characterized by 1D and 2D NMR experiments (Figures S1 and S2, Supporting Information).

Characteristics peaks for the phenyl carbonate (PhC) moiety disappeared in the spectra of CBzC and CCBzC. Most notably the peaks attributed to the carbonyl group of the carbonate moiety (153 ppm) and for the aromatic carbon atoms adjacent to the oxygen atom (150 ppm) and in *o*-position (121 ppm) were not present in the spectra of both reaction products. Thus, it can be concluded that PhC moieties were replaced quantitatively and that residual phenol that is formed as side product was fully removed. New peaks were identified that clearly indicate the formation of CBzC moieties, most notably the peaks ≈156 ppm (characteristic for the carbonyl group of a carbamate moiety) and 44 ppm (characteristic for the methylene group of a benzyl moiety). In addition, a new set of peaks in the aromatic region was detected with a peak ≈140 ppm, attributed to the carbon atom adjacent to the aliphatic methylene group. The spectrum obtained for CCBzC featured similar peaks indicating that the conversion of CPhC with 4-chlorobenzyl amine proceeded in an analog manner. An additional peak ≈131 ppm could be distinguished that was assigned to the aromatic carbon atom adjacent to the chlorin atom in *p*-position. Furthermore, it was observed that three individual peaks occurred that were related to the newly introduced carbonyl group of the carbamate moieties. Thus, functionalization occurred at positions C-2, C-3, and C-6. 2D-NMR experiments were performed but did not yield additional information because the spectra were mostly dominated by the peaks originating from the aromatic groups (Figure S2, Supporting Information). However, it should be pointed out that the overall DS values were quite

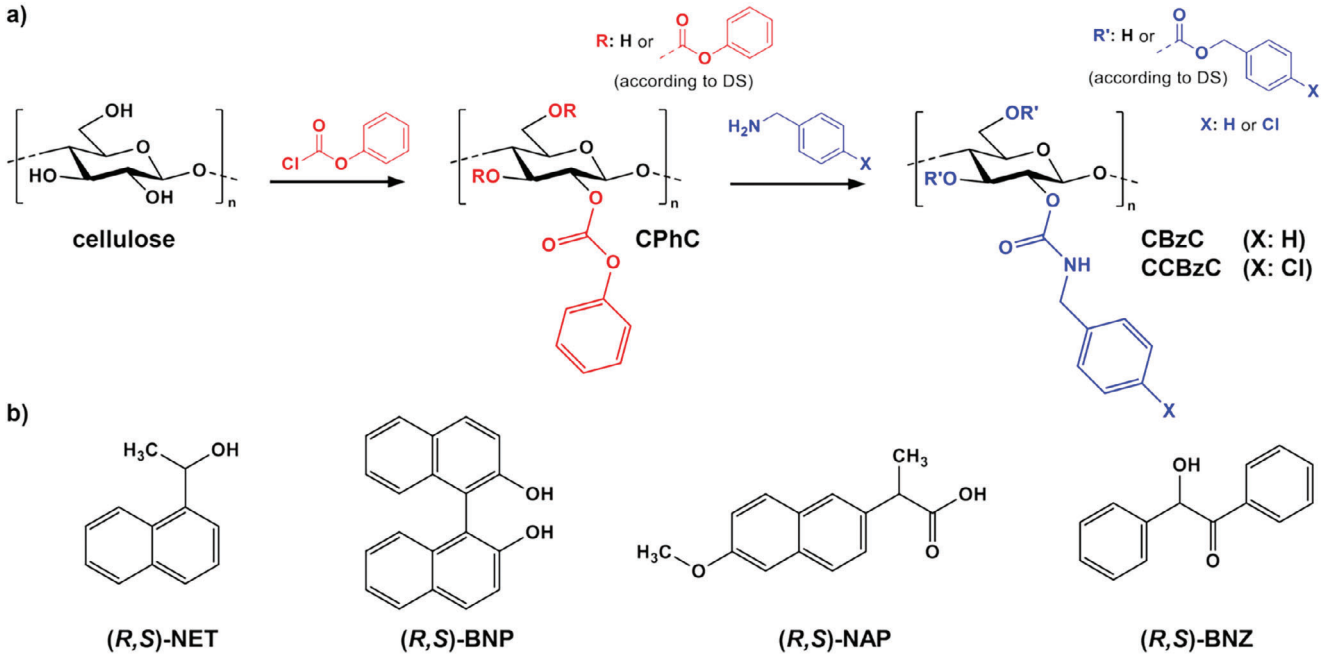

Figure 1. a) Reaction scheme for the synthesis of CPhC and the subsequent conversion into CBzC and CCBzC. b) Molecular structure of the racemic compounds used in this study.

high (≈2.5), i.e., the majority of the original hydroxy groups were converted, which results in a rather uniform distribution pattern. In a recent study on mixed polysaccharide carbamates that were prepared by the same modular synthesis strategy, 2D-NMR experiments could only provide limited qualitative information on the distribution pattern due to the lack of coupling cross-peaks between carbon atoms of the carbamate substituents with carbon atoms in the polysaccharide backbone.[34]

The DS values of 2.45 and 2.34 respectively determined for CBzC and CCBzC are slightly lower compared to the starting DS of CPhC. The DS values were derived from the nitrogen content of the two carbamate derivatives. This experimental approach is feasible and accurated because neither cellulose nor the CPhC starting materials contain nitrogen. Since no residual PhC groups were identified by NMR spectroscopy, it can be assumed that minor hydrolysis occurred during the conversion. Similar findings have been reported previously for the synthesis of other cellulose carbamates with high overall DS values using this modular synthesis approach.[30] Overall, it can be stated that the synthesis of aromatic cellulose carbamates was successful. Both derivatives readily dissolved in organic solvents such as acetone, *N,N*-dimethylformamide (DMF), tetrahydrofuran, *N,N*-dimethylacetamide, and 1,4-dioxane, which is a fundamental requirement for electrospinning. The polymeric nature of the compounds was confirmed by size exclusion chromatography (SEC), as shown in Figure S3 (Supporting Information) and the averaged molecular weights and the molecular weight distributions are listed in Table S1 (Supporting Information). The molecular weight of CCBzC is slightly smaller compared to CBzC probably because hydrolysis is slightly more pronounced during the synthesis of this compound. The reason for this is not entirely clear but it can be assumed that the impact on the electrospinning and membrane properties is low because the absolute differences are still quite small.

2.2. Electrospinning of the Cellulose Carbamates

For successful electrospinning, the volatility of the solvent to be used for the electrospinning was first adjusted. **Figure 2** shows optical microscope images of the electrospun products from CBzC solutions (16 wt%) in mixtures of DMF and acetone with different volume fractions. The electrospinning of the CBzC solution in pure DMF gave spherical bead-like products as shown in Figure 2a, probably due to the low volatility of the solvent that resulted in an unstable spray of the solution. Mixing higher volatile acetone to DMF improved the stability of the electrospinning process, forming a cone-like shaped structure of the solution on the tip of a needle-electrode, to form fibers coexistent with beads. The electrospinning from the mixture of acetone/DMF = 5/5 (v/v) gave large beads with thin fibers as shown in Figure 2b, while the one from acetone/DMF = 7/3 (v/v) gave smaller beads with thicker fibers as shown in Figure 2c. The product from the solution in acetone/DMF = 9/1 (v/v) gave the thickest fibers with almost no beads, while the electrospinning process was not stable because the solution was too highly volatile and quickly stuck within the needle-electrode by evaporation. Thus, we then studied the effect of concentration for the CBzC solution in the mixture of acetone/DMF = 7/3 (v/v).

Figure 3 shows scanning electron microscope (SEM) images of the electrospun products from the CBzC solutions in the mixture of acetone/DMF = 7/3 with various concentrations, and the histograms of the constituent fiber diameter distributions determined by statistical analysis of the SEM images. By increasing the

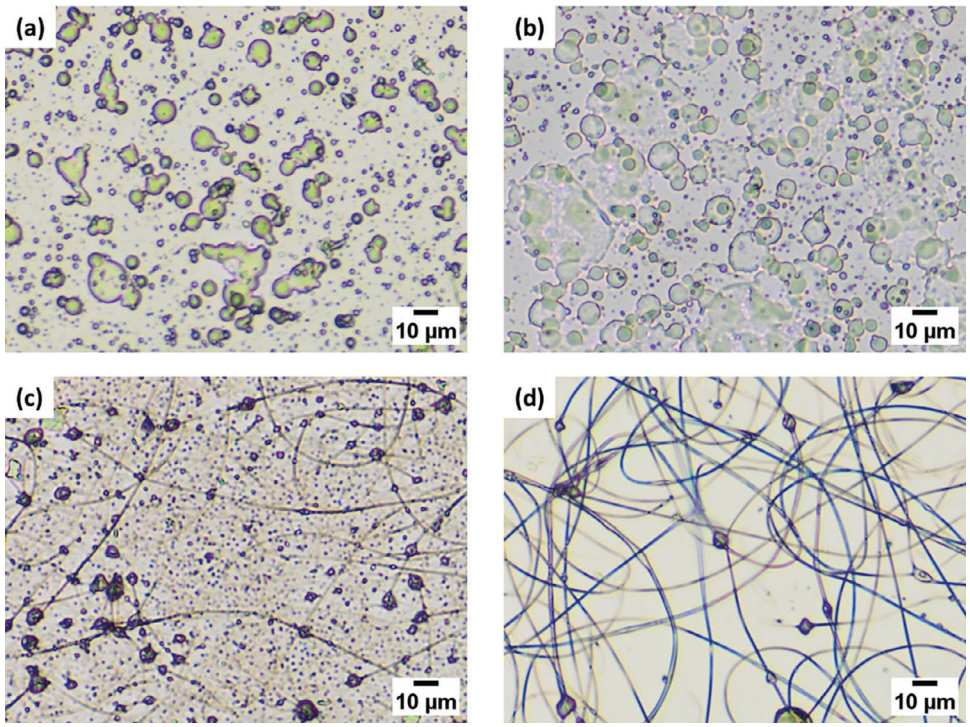

Figure 2. Optical microscope images of the electrospun products obtained from the CBzC solutions (16 wt%) in acetone/DMF (v/v) = a) 0/10: beads, b) 5/5: beads with thin fibers, c) 7/3: beads with thick fibers, and d) 9/1: thick fibers.

concentration from 16 to 22 wt% in steps of 2 wt%, obviously the fibers became thicker and the number of beads became smaller. This was confirmed by the increase of the mean fiber diameter (MD), i.e., the MD of 128 nm for the 16 wt % solution increased to 163, 203, and 315 nm for the 18, 20, and 22 wt% solutions, respectively. This type of phenomenon has been widely observed in the literature.[35,36] It can be explained by an increase in the viscosity with increase in the solution concentration due to the entanglement of the polymer chains, which results in the polymer solution being more resistant to the elongation force of the electric field. The electrospinning of the CCBzC solutions showed a similar trend as that of the CBzC solutions. Therefore, we prepared thick membranes of both CBzC and CCBzC from their solutions in acetone/DMF = 7/3 with 22 wt% for the study of their chiral resolution properties.

2.3. Enantioselective Permeations of Racemic Compounds Through the Membranes

The enantioselective permeation properties of the electrospun CBzC and CCBzC membranes were characterized by liquid–liquid permeation (LLP) experiments of the racemic compounds, (*R*,*S*)-NET, (*R*,*S*)-1,1′-bi-2-naphtol ((*R*,*S*)-BNP), (*R*,*S*)-naproxen ((*R*,*S*)-NAP), and (*R*,*S*)-benzoin ((*R*,*S*)-BNZ) as shown in **Figure 4**, through the membranes using a pair of "Side-By-Side" glass cells.[19] The solution of the racemic mixture placed in the left-side cell and the same volume of the pure eluent placed in the right-side cell separated by the membrane were gently stirred (Figure S4, Supporting Information), and a portion of the solution in the right-side cell was regularly sampled to determine *e.e.* (%) of a preferentially permeated enantiomer by the HPLC analysis. The *e.e.* values of the preferentially permeated enantiomers in the right-side cell were plotted against the time and shown in Figure 4a,b for the permeations using the membranes made of CBzC and CCBzC, respectively. Previously, we reported the enantioselective permeation of (*R*,*S*)-NET through the electrospun membranes made of CDMPC. In that study, the CDMPC membranes showed preferential permeation of (*S*)-NET, which was supported by higher binding energy via hydrogen bonding and π–π interactions between the chiral recognition cites of CDMPC and (*R*)-NET calculated by molecular docking simulation.[20] Herein, the CBzC membrane showed a reverse selectivity, i.e., preferential permeation of (*R*)-NET as shown in the blue plot in Figure 4a, while the CCBzC membrane showed the same selectivity as the CDMPC membranes, i.e., preferential permeation of (*S*)-NET as shown in the blue plot in Figure 4b. This suggests the molecular structures of the pendant groups of the cellulose-based CSs affect the enantioselectivity of the membranes as it is widely observed in the CSs used for the CSPs that are packed in the columns for HPLC. One notes that the *e.e.* values of the preferentially permeated (*R*)-NET and (*S*)-NET respectively through the CBzC and CCBzC membranes (≈1–2%) were smaller than those observed for (*S*)-NET permeated through the CDMPC membranes (≈3–16%). For (*R*,*S*)-BNP, both the CBzC and CCBzC membranes preferentially permeated (*S*)-BNP as shown in the green plots in Figure 4a,b. The *e.e.* values were slightly higher than those obtained for the separations of (*R*,*S*)-NET. For (*R*,*S*)-BNZ, the CBzC membrane did not show clear enantioselectivity (data not shown), while the CCBzC

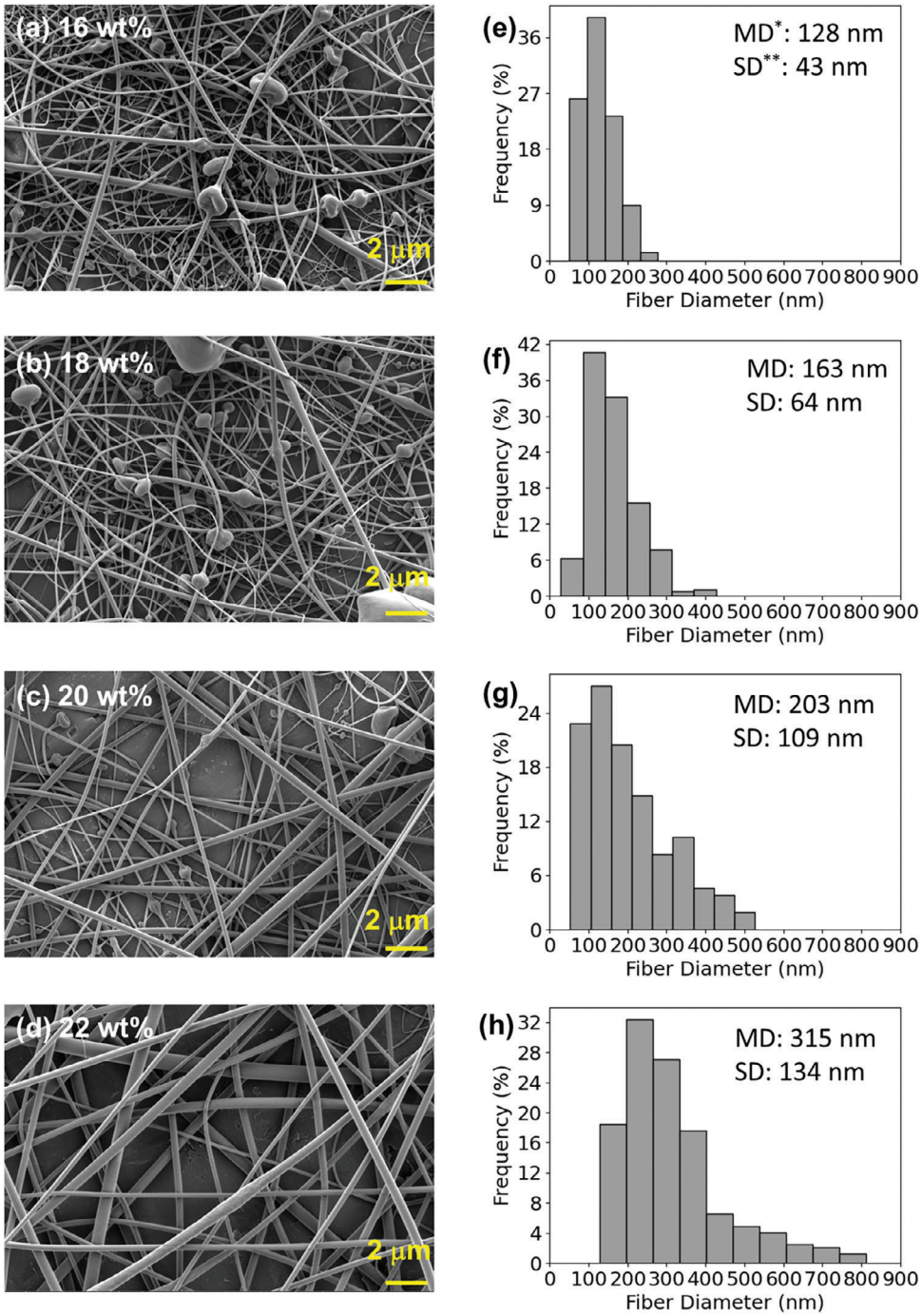

Figure 3. SEM images (left) and the corresponding histograms of diameter distributions (right) of the electrospun fibers from the CBzC solutions in the mixtures of acetone/DMF = 7/3 with 16 wt% (a and e), 18 wt% (b and f), 20 wt% (c and g), and 22 wt% (d and h). *MD: mean diameter. **SD: standard deviation.

membranes preferentially permeated (*S*)-BNZ with very small *e.e.* values (less than 1%) as shown in the red plot in Figure 4b. In contrast, the CCBzC membrane showed high enantioselectivity for the separation of (*R,S*)-NAP, i.e, (*R*)-NAP was preferentially permeated through the membrane with higher *e.e.* values (≈9–13%) as shown in the black plot in Figure 4b, while small *e.e.* values (≈1–2%) of (*R*)-NAP were observed using the CBzC membrane as shown in the black plot in Figure 4a. Such a drastic difference in enantioselectivity due to electron-donating/withdrawing substituent groups at the 4-position on the phenyl group were widely observed in cellulose carbamates-based CSPs used for chiral HPLC.[23] The averaged *e.e.* values obtained by the LLP experiments for each CS and racemic compound are summarized in Table S2 (Supporting Information).

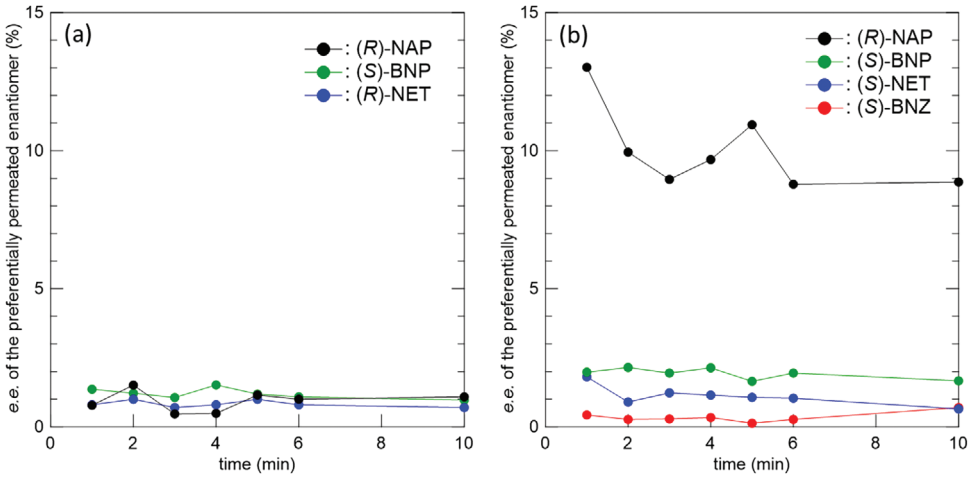

Figure 4. Plots of *e.e.* (%) of the preferentially permeated enantiomers though the electrospun membranes made of a) CBzC and b) CCBzC versus time of the permeation.

Most of the *e.e.* values were relatively small (*e.e.* < 2%) except for the separation of (*R,S*)-NAP using the CCBzC membrane (*e.e.* ≈ 10%). However, these small *e.e.* values were obtained by only a single permeation of the racemic compounds via natural diffusion through the membranes (i.e., the LLP method), and most importantly, they are not 0%. As we previously reported,[19] even though the *e.e.* values obtained by the LLP method are relatively small (but not 0%), they can be increased by repeating the filtration under pressure (for instance, by the vacuum filtration method). One notes that the *e.e.* values in the range of 1–10% in this study were generally observed in other membrane-based chiral resolutions using carbohydrate-based CSs that were reported recently (Table S3, Supporting Information).

Molecular docking simulations between the CSs and the enantiomers were performed in order to theoretically investigate the differences in the binding type, binding number, and binding free energies between the (*R*)-/(*S*)-enantiomers and the CSs through the enantioselective permeations at the molecular level. The energy and geometry of the interactions of CBzC and CCBzC with the enantiomers were studied by using AutoDock molecular modeling simulation software. The binding free energy (ΔG) which evaluates the thermodynamic stability of the complex of the CSs and the (*R*)-/(*S*)-enantiomers was calculated by a semi-empirical binding free energy function in the software. It should be noted that the docking simulations were done between the oligomers (degree of polymerization = 5) of the CSs and one single molecule of the enantiomers without the presence of the solvent in order to simplify the simulations. The 3D docking poses of CBzC and CCBzC with the enantiomers are shown in **Figures 5** and **6**, respectively. In addition, the type and number of the interactions between the CSs and the (*R*)- and (*S*)-enantiomers and the calculated ΔG values are listed in **Table 1**. As shown in Figure 5, CBzC interacts with (*R*)- and (*S*)-NET via different types and number of bindings, i.e., (*R*)-NET shows one hydrogen bonding interaction (green dotted line in Figure 5a) and three nonpolar (one π-alkyl and two π-sigma) interactions (purple dotted lines in Figure 5a), while (*S*)-NET shows two hydrogen bonding interactions (green dotted line in Figure 5b) without any nonpolar interaction as listed in Table 1 entries 1 and 2. As for the interactions of CBzC with (*R*)-/(*S*)-BNP, (*R*)-BNP shows two hydrogen bonding interactions (green dotted line in Figure 5c) and one nonpolar (π–π) interaction (purple dotted line in Figure 5c), while (*S*)-BNP shows only one hydrogen bonding interaction (green dotted line in Figure 5d) and one nonpolar (π–π) interaction (purple dotted line in Figure 5d) as listed in Table 1 entries 3 and 4. In case of the interactions with (*R*)-/(*S*)-NAP, (*R*)-NAP shows two hydrogen bonding interactions (green dotted lines in Figure 5e), while (*S*)-NAP shows one hydrogen bonding interaction (green dotted line in Figure 5f) and one nonpolar (π-alkyl) interaction (purple dotted line in Figure 5f) as listed in Table 1 entries 5 and 6. These differences in type and number of interactions should be the driving force of the preferential permeations of the enantiomers through the CBzC membrane observed in Figure 4a.

As shown in Figure 6, CCBzC interacts with (*R*)- and (*S*)-NET via different types and number of bindings, i.e., (*R*)-NET shows one hydrogen bonding interaction (green dotted line in Figure 6a), while (*S*)-NET shows two hydrogen bonding interactions (green dotted lines in Figure 6b) and two nonpolar (π-alkyl and π-sigma) interactions (purple dotted line in Figure 6b) as listed in Table 1 entries 7 and 8. Both (*R*)- and (*S*)-BNP interact with CCBzC via two hydrogen bonding interactions (green dotted lines in Figure 6c,d) and two nonpolar (π–π) interactions (purple dotted line in Figure 6c,d) as listed in Table 1 entries 9 and 10. Additionally, there is another noncovalent (π–Cl) interaction (pale purple dotted line in Figure 6d) between (*S*)-BNP and CCBzC (Table 1 entry 10). As for the interactions between CCBzC and (*R*)-/(*S*)-NAP, (*R*)-NAP shows one hydrogen bonding interaction (green dotted line in Figure 6e), two nonpolar (π-alkyl and π-sigma) interactions (purple dotted lines in Figure 6e), and one unfavorable interaction (red dotted line in Figure 6e) between oxygen atoms at the —CH_2—*O*— group of CCBzC and CH_3—*O*— group of (*R*)-NAP, while (*S*)-NAP shows two hydrogen bonding interactions (green dotted lines in Figure 6f), two nonpolar (π-alkyl and π-sigma) interactions (purple dotted lines in Figure 6f), and one unfavorable interaction (red dotted line in Figure 6f) between oxygen atoms at the —CH_2—*O*— group of CCBzC and CH_3—*O*— group of (*S*)-NAP as listed in Table 1 entries 11 and 12. Both (*R*)- and (*S*)-BNZ interact with CCBzC via one hydrogen

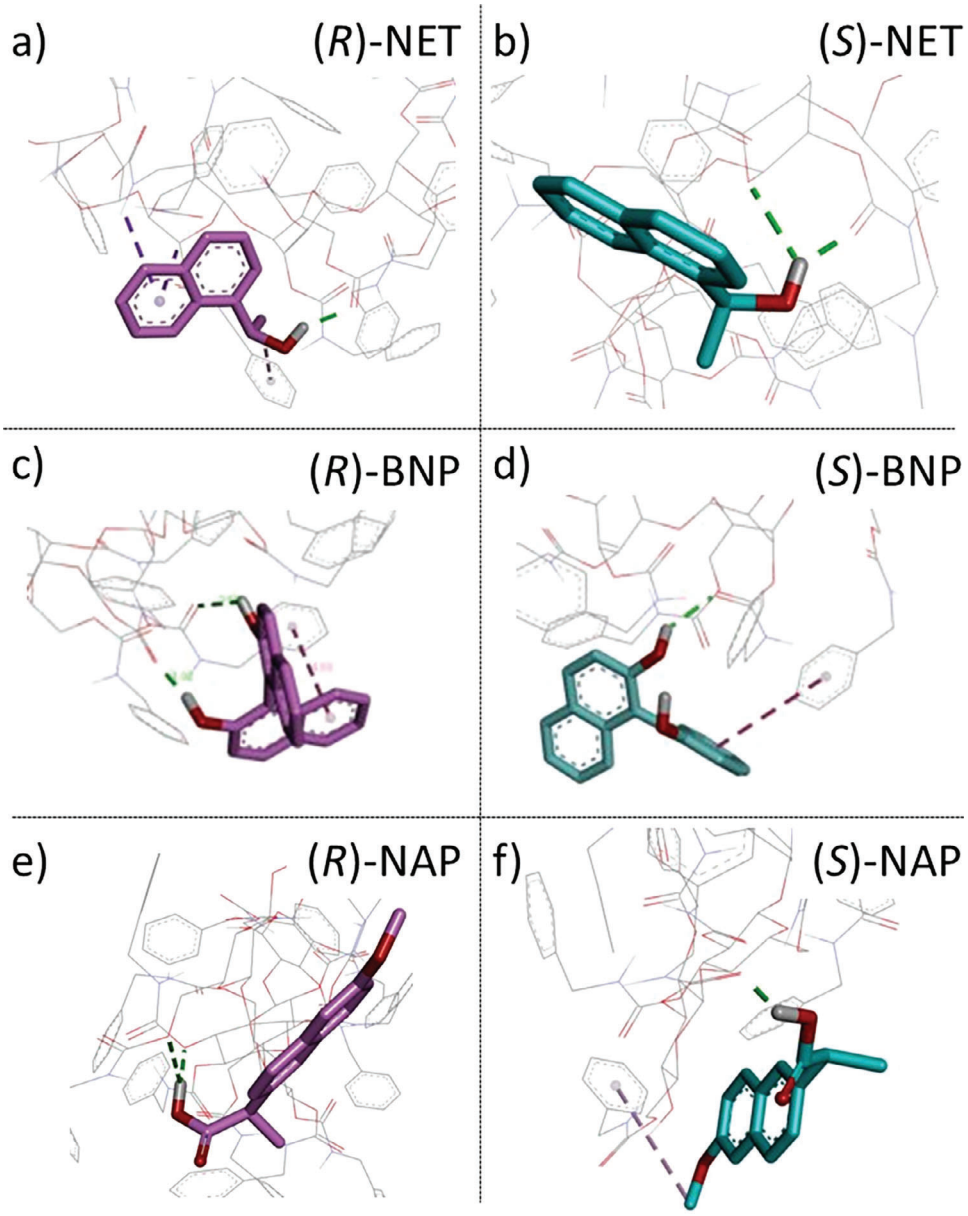

Figure 5. The 3D docking poses between CBzC and a) (*R*)-NET, b) (*S*)-NET, c) (*R*)-BNP, d) (*S*)-BNP, e) (*R*)-NAP, and f) (*S*)-NAP.

bonding interaction (green dotted lines in Figure 6g,h) and one nonpolar (π–π) interaction (purple dotted lines in Figure 6g,h), while two unfavorable interactions (red dotted lines in Figure 6h) between the oxygen atoms at the carbonyl oxygen of (*S*)-BNZ and the —CH_2—*O*— group of CCBzC as well as the carbamate group of CCBzC are observed as listed in Table 1 entries 13 and 14. These differences in type and number of interactions should be the driving force of the preferential permeations of the enantiomers through the CCBzC membrane observed in Figure 4b.

As listed in Table 1, the ΔG values between the two CSs and all the enantiomers investigated here were negative, indicating that the retentions of the enantiomers by the chiral recognition sites of the CSs are spontaneous processes.[37,38] For each enantiomer, the ΔG values of the interactions with the (*R*)- and (*S*)-enantiomers were different as listed in the column of $|\Delta\Delta G|$, that is, the absolute value of the difference of ΔG between the (*R*)- and (*S*)-enantiomer. On the one hand, the difference in ΔG supports the experimental results of the enantioselective permeations of (*R*)-/(*S*)-BNP through the membranes made of CBzC and CCBzC. In the case of CBzC, the higher negative ΔG value for (*R*)-BNP ($\Delta G = -5.24$ kcal mol^{-1} shown in entry 3) than that for (*S*)-BNP ($\Delta G = -5.01$ kcal mol^{-1} shown in entry 4) indicates stronger retention of (*R*)-BNP than (*S*)-BNP, which is in good agreement with the preferential permeation of (*S*)-BNP as shown in Figure 4a. In the same way, the preferential permeation of (*S*)-BNP through the CCBzC membrane shown in Figure 4b was supported by the higher negative ΔG value for (*R*)-BNP ($\Delta G = -5.86$ kcal mol^{-1} shown in entry 9) than that for (*S*)-BNP

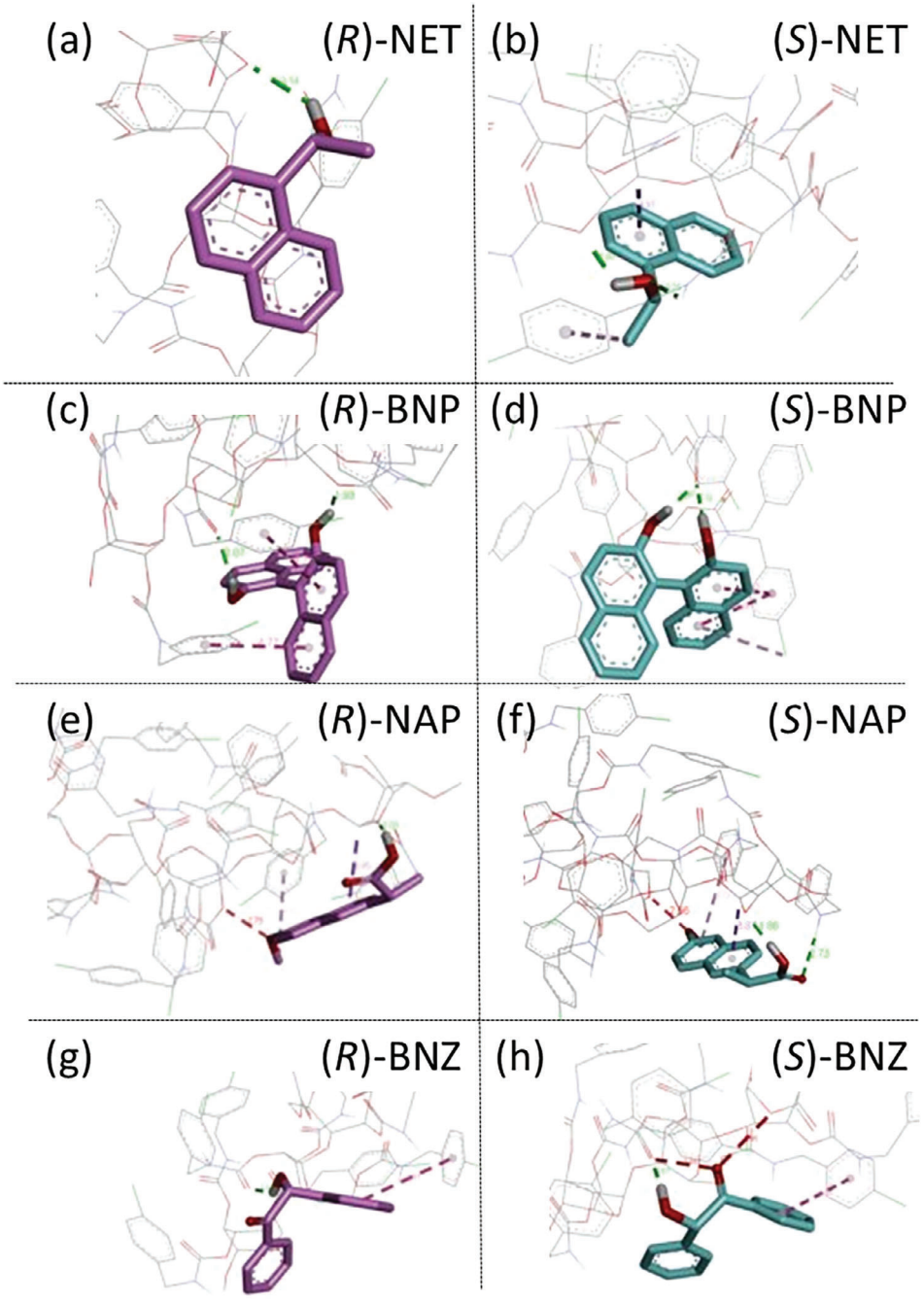

Figure 6. The 3D docking poses between CCBzC and a) (*R*)-NET, b) (*S*)-NET, c) (*R*)-BNP, d) (*S*)-BNP, e) (*R*)-NAP, f) (*S*)-NAP, g) (*R*)-BNZ, and h) (*S*)-BNZ.

(ΔG = −5.82 kcal mol^{-1} shown in entry 10). The preferential permeation of (*R*)-NAP through the CBzC membrane was also supported by the higher negative ΔG value for (*S*)-NAP (ΔG = −4.29 kcal mol^{-1} shown in entry 6) than that for (*R*)-NAP (ΔG = −4.26 kcal mol^{-1} shown in entry 5). On the other hand, the experimental results were not supported by the calculated ΔG values for the other enantiomers. For example, the higher negative ΔG value for (*R*)-NET (ΔG = −4.62 kcal mol^{-1} shown in entry 1) than that for (*S*)-NET (ΔG = −4.52 kcal mol^{-1} shown in entry 2) indicates stronger retention of (*R*)-NET than (*S*)-NET, which does not support the preferential permeation of (*R*)-NET through the CBzC membrane as shown in Figure 4a, while the preferential permeation of (*S*)-NET through the CCBzC membrane shown in Figure 4b are in good agreement with the higher negative ΔG value for (*R*)-NET (ΔG = −5.49 kcal mol^{-1} shown in entry 7) than that for (*S*)-NET (ΔG = −5.45 kcal mol^{-1} shown in entry 8). One can assume that such contradictory results of the calculations represent the very low enantioselectivities (*e.e.* = ≈1–2%)

Table 1. The results of the molecular docking between the CSs (CBzC and CCBzC) and the different enantiomers.

Entry	CSs	Enantiomers	ΔG [kcal mol^{-1}]	Number of H-bonding interactions	Number of nonpolar interactions	Other forms of interactions	Unfavorable interactions	$\lvert\Delta\Delta G\rvert$[a)] [kcal mol^{-1}]
1	CBzC	(*R*)-NET	−4.62	1	3	0	0	0.10
2		(*S*)-NET	−4.52	2	0	0	0	
3		(*R*)-BNP	−5.24	2	1	0	0	0.23
4		(*S*)-BNP	−5.01	1	1	0	0	
5		(*R*)-NAP	−4.26	2	0	0	0	0.03
6		(*S*)-NAP	−4.29	1	1	0	0	
7	CCBzC	(*R*)-NET	−5.49	1	0	0	0	0.04
8		(*S*)-NET	−5.45	2	2	0	0	
9		(*R*)-BNP	−5.86	2	2	0	0	0.04
10		(*S*)-BNP	−5.82	2	2	1	0	
11		(*R*)-NAP	−4.60	1	2	0	1	0.05
12		(*S*)-NAP	−4.55	2	2	0	1	
13		(*R*)-BNZ	−4.70	1	1	0	0	0.01
14		(*S*)-BNZ	−4.71	1	1	0	2	

[a)] Absolute value of the difference of free binding energy (ΔG) between the (*R*)- and (*S*)-enantiomer.

of both CBzC and CCBzC to (*R*)-/(*S*)-NET. The calculated ΔG values for the interactions of CCBzC with (*R*)-/(*S*)-NAP shown in entries 11/12 and (*R*)-/(*S*)-BNZ shown in entries 13/14 did not support the experimental results. Unlike other cases, unfavorable interactions between the oxygen atoms at the CSs and the enantiomers were observed for these docking simulations, which can be one of the reasons for the unsubstantiated calculations. It is worth noting that the molecular docking simulations provide insight into static molecular interactions between the CSs whose 3D structures were kept rigid after energy minimization and the enantiomers without solvents but not into the actual diffusion behaviors of the enantiomers within the membranes. This means that the dynamic nature of the interaction between the CSs in the membranes and the enantiomers such as swelling of both the CSs and the enantiomers in solvents[39] should be taken into consideration for more reliable theoretical investigations toward a mechanism elucidation of chiral resolutions.

3. Conclusion

Two cellulose derivatives, namely CBzC and CCBzC were synthesized using a modular approach. Self-standing nanofibrous membranes of CBzC and CCBzC could be prepared by electrospinning as the new type of enantioselective membranes. The enantioselectivity of these membranes was characterized by the LLP experiments using four racemic compounds, (*R*,*S*)-NET, (*R*,*S*)-BNP, (*R*,*S*)-NAP, and (*R*,*S*)-BNZ. Both the CBzC and CCBzC membranes showed enantioselective permeations of (*R*)-/(*S*)-NET ((*R*)-NET through the CBzC membrane and (*S*)-NET through the CCBzC membrane), (*S*)-BNP, and (*R*)-NAP. Notably, the membrane made of CCBzC, whose enantiorecognition has never been reported, showed enantioselective permeation of (*R*)-NAP with high *e.e.* values (≈9–13%). The molecular docking simulations of CBzC and CCBzC with the enantiomers indicated different types of interactions such as hydrogen bonding, π–π, π–alkyl, π–sigma, π–Cl interactions, as well as some unfavorable interactions between the oxygen atoms, which can be the driving force of the enantioselective permeations although the calculated ΔG did not fully support the experimental results probably due to the limitation of the docking for static molecular interactions without solvents.

4. Experimental Section

Materials: Avicel PH-101 microcrystalline cellulose (≈50 µm particle size) was purchased from Sigma–Aldrich Co. and dried overnight under vacuum at 60 °C prior to use. ((*R*,*S*)-NAP) (>98.0%) was purchased from Tokyo Chemical Industry Co. ((*R*,*S*)-BNZ) (≥99%) was purchased from Thermo Scientific Chemicals. Acetone (≥99.8%) and DMF (≥99.9%) were purchased from Carlo Erba Co. ((*R*,*S*)-BNP) (99%), (*R*,*S*)-NET (≥99%), *n*-hexane for HPLC (≥95%), 2-propanol for liquid chromatography (≥99.9%), trifluoroacetic acid (≥99.0%), and 1-butyl-3-methylimidazolim chloride (BMIMCl) (≥98.0%) were purchased from Sigma–Aldrich Co. Unless specified otherwise, all chemicals were used as received by the supplier.

Instruments: The NMR spectra were recorded with a Bruker Avance 250 MHz or a Bruker Avance 400 MHz spectrometer at concentrations of 50 mg mL^{-1}. A VARIO EL III CHNS analyzer (Elementaranalysensysteme GmbH) was used to determine the elemental composition. The DS with phenyl carbonate groups was determined by ^{1}H-NMR spectroscopy.

Thereby, trifluoroacetic acid (≈15 drops) was added to the polymer solution to shift the water peak. The DS values of the carbamate derivatives were determined by elemental analysis (see the supporting information). SEC was performed with an Agilent Technologies 1260 Infinity Multi Detector Suite GPC/SEC System equipped with a refractive index (RI) detector, an ultraviolet (UV) detector, a dual-angle (90° and 15°) light scattering (LS) detector, and a set of columns (Shodex Asahipak GF-1G 7B, GF-7 M HQ, and GF-310 HQ) operating at 40 °C using DMF containing 0.01 M LiCl as an eluent at a flow rate of 0.6 mL min^{-1}. A Wyatt Optilab rEx differential RI detector was used to determine dn/dc values. The number-average molecular weight (M_n), weight-average molecular weight (M_w), and molecular weight dispersity ($Đ_M = M_w/M_n$) of CBzC and CCBzC were determined by absolute molecular weight analysis using the LS detector. Electrospinning was performed with a Fuence Esprayer ES-2000S2A. The optical microscope images were observed by a ZEISS Axiophot II microscope and recorded with an Olympus SC50 digital camera operated by Olympus Stream software. The SEM images of the specimens coated with a ≈4 nm-thick layer of gold/palladium (Au/Pd) were observed by a FEI QUANTA FEG 250 microscope operating at an accelerating voltage of 2.5 kV. HPLC was performed with a Thermo Fisher Scientific UltiMate 3000 HPLC system equipped with a VWD-3100 UV (λ = 270 and 230 nm) detector and a Daicel CHIRALPAK IB N-3 (length × inner diameter: 100 × 4.6 mm, particle size: 3 µm) analytical column operating at 30 °C using a mixed solvent of *n*-hexane and 2-propanol (*n*-hexane/2-propanol = 9/1 (v/v)) for (*R*,*S*)-NET, (*R*,*S*)-BNP, and (*R*,*S*)-BNZ, and a mixed solvent of *n*-hexane, 2-propanol, and trifluoroacetic acid (*n*-hexane/2-propanol/trifluoroacetic acid = 95/5/0.1 (v/v/v)) for (*R*,*S*)-NAP as eluents at a flow rate of 1.0 mL min^{-1}. and data were processed using Chromeleon software (Ver. 7.2.10).

Synthesis of CPhC: The synthesis was performed under homogeneous reaction conditions as previously described.[30] Cellulose (75 g, 462.68 mmol) was mixed with BMIMCl (675 g) and stirred at 80 °C for ≈2 h upon which melting of the ionic liquid occurred. Pyridine (350 mL) was added dropwise over a timeframe of 1 h and the mixture was stirred at 80 °C for 20 h, which yielded an optically clear viscous solution. The solution was cooled to 25 °C and pyridine (350 mL) was added dropwise over a timeframe of 1 h during the cooling. Phenyl chloroformate (290 g, 1852.20 mmol) was added dropwise within 1 h and the mixture was stirred for another 3 h keeping the reaction temperature at 25 °C using a thermostat. Afterward, the reaction mixture was poured into water (15 L) and the precipitate formed was removed by filtration, washed four times with ethanol (4 L each), and dried at 50 °C under vacuum to obtain the final product.

DS: 2.88. ^{13}C-NMR (63 MHz, DMSO-d_6, δ): 152.6 (C-7), 150.6 (C-8), 129.7 (C-10), 126.2 (C-2), 121.0 (C-9), 99.6 (C-1), 76.8-67.2 (C-2 to C-6) ppm.

Synthesis of CBzC and CCBzC: For the preparation of CCBzC, CPhC (12.0 g; mmol) was dissolved in DMF (150 mL) at 60 °C. 4-Chlorobenzyl amine (39.40 g, 278.25 mmol, 4 mol/mol phenyl carbonate (PhC) groups) was added and the mixture was stirred for 20 h at 60 °C. Afterward, the product was isolated by precipitation in ethanol (1 L), washed with ethanol (three times with 300 mL) and dried at 50 °C under vacuum. CBzC was prepared in an analogue manner but using benzyl amine instead of 4-chlorobenzyl amine.

CBzC:

DS: 2.45. Elemental composition: found: C% 62.39, H% 5.63, N% 7.03, calculated: C% 62.99, H% 5.56, N% 7.03. ^{13}C-NMR (63 MHz, DMSO-d_6, δ): 156.9–155.4 (C-12), 139.5 (C-14), 128.2 (C-17), 127.0–126.7 (C-15 and C-16), 100.5 (C-1), 78.0–65.0 (C-2 to C-6), 44.1 (C-13) ppm.

CCBzC:

DS: 2.34. Elemental composition: found: C% 52.19, H% 4.16, N% 5.92, calculated: C% 53.38, H% 4.34, N% 5.92. ^{13}C-NMR (63 MHz, DMSO-d_6, δ): 156.8–155.6 (C-12), 138.4.5 (C-14), 131.2 (C-17), 128.2 (C-15 and C-16), 100.5 (C-1), 78.0–65.0 (C-2 to C-6), 43.0 (C-13) ppm.

Electrospinning: A typical electrospinning procedure is as follows: CBzC (500 mg) was dissolved in 1.9 g of a mixed solvent of acetone and DMF (acetone/DMF = 7/3 (v/v)) for 24 h by stirring using a magnetic stirrer. The obtained solution was inserted into two 5 mL syringes equipped with needles (Nordson stainless steel tips 18 gauge; inner diameter = 0.84 mm, outer diameter = 1.27 mm) that were placed 15 cm away from a metallic electrode plate (20 cm × 20 cm square) covered with aluminum foil. A high voltage of 25 kV was applied between the needles and the electrode plate while the solution was delivered at a feed rate of 30 µL min^{-1} at room temperature (≈25 °C) and humidity (≈30%). To ensure that the fibers are electrospun evenly over the whole surface of the aluminum foil, the electrode plate was continually moved while its center drew a 5 cm × 5 cm square, which was controlled by a computer program.

Chiral Separation: Chiral separations of the racemic compounds were performed by LLP experiments.[19] A typical LLP experiment is as follows: An electrospun CBzC membrane collected on an aluminum foil was cut into a small piece (≈3 cm × 3 cm square) and the membrane was carefully peeled off from the aluminum foil using tweezers. The peeled membrane was sandwiched between two Whatman polytetrafluoroethylene (PTFE) membrane filters (pore size: 1 µm, diameter: 47 mm) as a support of the membrane. The membrane was arranged between a pair of 15 mm unjacketed "Side-Bi-Side" glass cells (PermeGear Inc.) equipped with magnetic stirring bars in each cell. A 5 mL solution of (*R*,*S*)-NET in a mixed solvent of *n*-hexane and 2-propanol (*n*-hexane/2-propanol = 9/1 (v/v)) (2 g L^{-1}) was placed in the left-side cell and 5 mL of the eluent was placed in the right-side cell. The solutions in both cells were stirred at room temperature (≈25 °C) and 150 µL of the solution in the right-side cell was sampled every minute. The sample solutions containing permeated (*R*)- and (*S*)-NET from the right-side cell were analyzed by the HPLC equipped with a CDMPC packed column (Daicel CHIRALPAK IB N-3). The enantiomeric excess (*e.e.*) values (%) of the samples (e.g., in the cases of preferential permeations of the (*S*)-enantiomers) were determined by comparing the two independent peak areas of the (*S*)-enantiomer and the (*R*)-enantiomer from the HPLC chromatograms according to the following equation[40]:

$$e.e.\ (\%) = \frac{A_S - A_R}{A_S + A_R} \times 100 \quad (1)$$

where A_S and A_R are the peak areas of the (*S*)-enantiomer and the (*R*)-enantiomer in the chromatogram, respectively. The chiral separations of the other racemic compounds were performed by the same procedure. For the LLP of (*R*,*S*)-NAP, a mixed solvent of n-hexane, 2-propanol, and trifluoroacetic acid (n-hexane/2-propanol/trifluoroacetic acid = 95/5/0.1 (v/v/v)) was used as the eluent.

Molecular Construction and Docking Simulations: Molecular docking simulations were done on an Intel Celeron CPU (2.80 GHz) and a Microsoft Windows 10 Pro operating system. The 2D structures of the ligands and receptors were sketched on ChemBioDraw Ultra (12.0 version) and transformed to 3D using ChemBio3D Ultra (12.0 version). The 3D structures were then energy minimized using the MM2 energy minimization algorithm of ChemBio3D. The ligands used in this study were the (*R*)- and (*S*)-enantiomers of NET, BNP, NAP, and BNZ while the receptors were CBzC and CCBzC. Autodock Tools (ADT) 1.5.7. was used for the processing of the receptors and the ligands before docking. The Kollman and Gasteiger charges were computed for the receptors, while for the ligands Gasteiger charges and rotatable bonds were assigned before saving them in PDBQT format. A grid box of 126 × 64 × 62 Å with a spacing of 0.375 Å was used. The ligands were treated as flexible while the receptors were kept rigid in the docking protocol. Docking was executed with Autodock 4.2 with 100 docking runs using the Lamarckain genetic algorithm (LGA). The default setting was used for all other docking parameters. The ligands–receptors interactions and scoring functions were used to choose the docked structures and for further analysis. Results differing by less than 2 Å in a positional all atom-based root mean square deviation (RMSD) were clustered together. The average binding free energy was calculated according to the following equation[41,42]:

$$E = \sum_{i=1}^{n} (E_i \times X_i) \quad (2)$$

where E is the average binding free energy, n is the number of conformational clusters, E_i is the binding free energy of this cluster conformation, X_i is the percentage frequency of this cluster conformation. The greater negative values of the binding energy reflect the greater stability of the enantiomer–CSs binding.

Supporting Information

Supporting Information is available from the Wiley Online Library or from the author.

Acknowledgements

This study was financially supported by the French National Research Agency "ChiralCell" project (ANR-23-CE06-0018). I.O. is grateful for a grant "Emergence International" by the Institute of Chemistry (INC) of the National Centre for Scientific Research (CNRS) which supported his research visit to Friedrich-Schiller-University of Jena to initiate this collaborative research. I.O. also thanks "International Research Booster" in the framework of the "Investissements d'avenir" program (ANR-15-IDEX-02) by Université Grenoble Alpes. T.H. is indebted to the funding received by the German Federal Ministry of Food and Agriculture, based on an enactment of the German Bundestag (2220NR252X). The authors acknowledge Dr. C. Lancelon-Pin of the ICMG Platform-Grenoble for the SEM observation, and Ms. L. Buon, Ms. C. Billet, and Mr. E. Bayma for the HPLC and dn/dc analysis at the Chromatography and Sugar Analysis Platform (PCANS) of the CERMAV. The authors are thankful to Prof. R. Pecora (Stanford University), Dr. Y. Ogawa, Dr. Y. Nishiyama, and Dr. J.-L. Putaux (CERMAV) for fruitful discussions.

Conflict of Interest

The authors declare no conflict of interest.

Author Contributions

S.N.-T. performed formal analysis, investigation, validation, visualization, and writing – original draft. T.H. performed funding acquisition, supervision, validation, and writing – review and editing. M.G. performed formal analysis, investigation, resources, supervision, validation, writing – review and editing. I.O. performed conceptualization, funding acquisition, methodology, project administration, supervision, validation, and writing – review and editing.

Data Availability Statement

The data that support the findings of this study are available from the corresponding author upon reasonable request.

Keywords

cellulose carbamates, chiral resolution, electrospinning, enantioselective membranes, molecular docking, nanofibers

Received: August 27, 2024
Revised: October 20, 2024
Published online:

[1] P. Vedovello, C. Marcio Paranhos, C. Fernandes, M. E. Tiritan, *Sep. Purif. Technol.* **2022**, *280*, 119800.
[2] N. M. Maier, P. Franco, W. Lindner, *J. Chromatogr. A* **2001**, *906*, 3.
[3] E. R. Francotte, *J. Chromatogr. A* **2001**, *906*, 379.
[4] P. G. McGarraugh, S. E. Brenner-Moyer, *Org. Lett.* **2011**, *13*, 6460.
[5] F. Zhou, O. Shemchuk, M. D. Charpentier, C. Matheys, L. Collard, J. H. ter Horst, T. Leyssens, *Angew. Chem., Int. Ed.* **2021**, *60*, 20264.
[6] W. Chen, X. Qiu, Y. Chen, X. Bai, H. Liu, J. Ke, Y. Ji, J. Chen, *Sep. Purif. Technol.* **2023**, *327*, 124898.
[7] F. F. Huerta, A. B. E. Minidis, J.-E. Bäckvall, *Chem. Soc. Rev.* **2001**, *30*, 321.
[8] R. Xie, L.-Y. Chu, J.-G. Deng, *Chem. Soc. Rev.* **2008**, *37*, 1243.
[9] T. Liu, Z. Li, J. Wang, J. Chen, M. Guan, H. Qiu, *Chem. Eng. J.* **2021**, *410*, 128247.
[10] L. Persano, A. Camposeo, C. Tekmen, D. Pisignano, *Macromol. Mater. Eng.* **2013**, *298*, 504.
[11] A. Greiner, J. H. Wendorff, *Angew. Chem., Int. Ed.* **2007**, *46*, 5670.
[12] M. Yoshikawa, K. Tharpa, Ş.-O. Dima, *Chem. Rev.* **2016**, *116*, 11500.
[13] M. Yoshikawa, K. Nakai, H. Matsumoto, A. Tanioka, M. D. Guiver, G. P. Robertson, *Macromol. Rapid Commun.* **2007**, *28*, 2100.
[14] Y. Sueyoshi, A. Utsunomiya, M. Yoshikawa, G. P. Robertson, M. D. Guiver, *J. Membr. Sci.* **2012**, *401–402*, 89.
[15] H. Mizushima, M. Yoshikawa, N. Li, G. P. Robertson, M. D. Guiver, *Eur. Polym. J.* **2012**, *48*, 1717.
[16] T. Kawasaki, M. Yoshikawa, *Desalination Water Treatment* **2013**, *51*, 5080.
[17] K. Shiomi, M. Yoshikawa, *Sep. Purif. Technol.* **2013**, *118*, 300.
[18] K. Shiomi, M. Yoshikawa, *J. Membr. Sep. Technol.* **2016**, *5*, 103.
[19] I. Otsuka, K. Pandey, H. Ahmadi-Nohadani, S. Nono-Tagne, *ACS Macro Lett.* **2021**, *10*, 921.
[20] S. Nono-Tagne, Y. Navon, Y. Ogawa, B. Carré, I. Otsuka, *Cellulose* **2024**, *31*, 2765.
[21] G. Hesse, R. Hagel, *Chromatographia* **1973**, *6*, 277.
[22] Y. Okamoto, E. Yashima, *Angew. Chem., Int. Ed.* **1998**, *37*, 1020.
[23] T. Ikai, Y. Okamoto, *Chem. Rev.* **2009**, *109*, 6077.
[24] Y. Okamoto, *Proc. Japan Academy* **2015**, *91*, 246.
[25] Y. Okamoto, M. Kawashima, K. Hatada, *J. Chromatogr. A* **1986**, *363*, 173.
[26] Y. Okamoto, R. Aburatani, T. Fukumoto, K. Hatada, *Chem. Lett.* **1987**, *16*, 1857.
[27] Y. Kaida, Y. Okamoto, *J. Chromatogr. A* **1993**, *641*, 267.
[28] T. Elschner, T. Heinze, *Macromol. Biosci.* **2015**, *15*, 735.
[29] L. Gabriel, M. Gericke, T. Heinze, *Carbohydr. Polym.* **2019**, *207*, 782.
[30] M. Gericke, Z. Atmani, L. H. Skodda, T. Heinze, *Carbohydrate Polym. Technol. Appl.* **2024**, *7*, 100479.
[31] C. V. Bui, T. Rosenau, H. Hettegger, *Cellulose* **2023**, *30*, 153.
[32] C. V. Bui, T. Rosenau, H. Hettegger, *Cellulose* **2023**, *30*, 2337.
[33] T. Elschner, M. Kötteritzsch, T. Heinze, *Macromol. Biosci.* **2014**, *14*, 161.
[34] M. Gericke, Z. Atmani, L. H. Skodda, T. Heinze, *Carbohydrate Polym. Technol. Appl.* **2024**, *7*, 100479.
[35] H. Lee, M. Nishino, D. Sohn, J. S. Lee, I. S. Kim, *Cellulose* **2018**, *25*, 2829.
[36] A. S. Motamedi, H. Mirzadeh, F. Hajiesmaeilbaigi, S. Bagheri-Khoulenjani, M. Shokrgozar, *Prog. Biomater.* **2017**, *6*, 113.
[37] Y. Li, D. Liu, P. Wang, Z. Zhou, *J. Sep. Sci.* **2010**, *33*, 3245.
[38] Y. Yao, P. Song, X. Wen, M. Deng, J. Wang, X. Guo, *J. Sep. Sci.* **2017**, *40*, 2999.
[39] R. B. Kasat, Y. Zvinevich, H. W. Hillhouse, K. T. Thomson, N.-H. L. Wang, E. I. Franses, *J. Phys. Chem. B* **2006**, *110*, 14114.
[40] J. H. Kim, J. H. Kim, J. Jegal, K.-H. Lee, *J. Membr. Sci.* **2003**, *213*, 273.
[41] J. Ke, K. Yang, X. Bai, H. Luo, Y. Ji, J. Chen, *Sep. Purif. Technol.* **2021**, *255*, 117717.
[42] H. Luo, X. Bai, H. Liu, X. Qiu, J. Chen, Y. Ji, *Sep. Purif. Technol.* **2022**, *285*, 120336.